Chin. J. Astron. Astrophys. Vol. 7 (2007), No. 4, 601–610
(*http://www.chjaa.org*)

Chinese Journal of
Astronomy and
Astrophysics

A Survey of Newtonian Core-Shell Systems with Pseudo High Order Symplectic Integrator and Fast Lyapunov Indicator *

Jun-Fang Zhu, Xin Wu and Da-Zhu Ma

Department of Physics, Nanchang University, Nanchang 330031; *xwu@ncu.edu.cn*

Received 2006 December 22; accepted 2007 April 27

Abstract Newtonian core-shell systems, as limiting cases of relativistic core-shell models under the two conditions of weak field and slow motion, could account for massive circumstellar dust shells and rings around certain types of star remnants. Because this kind of systems have Hamiltonians that can be split into a main part and a small perturbing part, a good choice of the numerical tool is the pseudo 8th order symplectic integrator of Laskar & Robutel, and, to match the symplectic calculations, a good choice of chaos indicator is the fast Lyapunov indicator (FLI) with two nearby trajectories proposed by Wu, Huang & Zhang. Numerical results show that the FLI is very powerful when describing not only the transition from regular motion to chaos but also the global structure of the phase space of the system.

Key words: celestial mechanics — chaos — methods: numerical

1 INTRODUCTION

Chaos, or deterministic unpredictable behavior of nonlinear dynamical systems, has been of great interest in dynamical astronomy (Contopoulos & Barbanis 1989; Wu & Zhang 2006; Wu et al. 2006b). There are two factors that affect the reliability of the identification of chaos for a given system. One depends on numerical algorithms. As is well-known, the traditional integrators with artificial dissipation in long-term numerical integrations can cause a great bias from some invariant manifolds so that results of the calculations are unreliable. However, the integrators combined with the manifold correction technique of Nacozy (1971) or Baumgarte (1973) may remedy the defect. Note, as a crucial point, we should be very careful when using this kind of manifold correction. Wu et al. (2006c) pointed out that it is very important to control both of the two independent energy integrals rather than just the total energy for an autonomous Hamiltonian system separable into two constant pieces. Further, this idea was extended to Hamiltonian systems involving many constraints (Wu & He 2006), and an n-body problem with $n-1$ varying Kepler energies in the solar system (Wu et al. 2007). Clearly, these numerical schemes with the manifold corrections do not maintain the symplectic structure of Hamiltonian systems, but symplectic integrators do. In this sense, symplectic integrators are regarded as an adaptive tool for the qualitative study of long-term evolution. The most popular method is the second-order leapfrog symplectic integrator of Wisdom & Holman (1991), in which the Hamiltonian is separated into a Keplerian part and an interaction one. It is said that the computation efficiency of the symplectic scheme has been improved dramatically. Especially the merit of the pseudo-high-order symplectic integrators (Chambers & Murison 2000; Laskar & Robutel 2001; Liu et al. 2005) has become more manifest than that of the corresponding conventional symplectic integrators of Yoshida (1990). Thus, the pseudo-order integrators are worth recommending when the Hamiltonian system is of a similar separable form.

The other factor concerns chaos indicators. Each of the known chaos indicators has its advantages and shortcomings. The Poincaré surfaces of section are the most common qualitative tool in the analysis of

* Supported by the National Natural Science Foundation of China.

dynamical systems, but they are most useful only when the number of degrees of freedom minus the number of constraints is not larger than two. For a system of many degrees of freedom, the Lyapunov characteristic exponents (LCEs), which measure the average exponent diverge rate of the distance between two adjacent orbits in the phase space, are perhaps a better choice. A compact system is ordered (i.e., stable periodic, or quasiperiodic) if its maximal LCE is zero, and chaotic if the LCE is positive. There are two different paths for calculating the LCE: the variational method and the two-particle method (Tancredi et al. 2001). The former involves solving the variational equations together with the equations of motion, while the latter needs only the integration of two nearby orbits that start very close to each other. In this case, it is necessary to use an appropriate initial distance between the two nearby orbits and an appropriate interval between successive renormalizations. It has been emphasized that the LCEs defined in the configuration space are completely equivalent to ones given in the phase space (Wu & Huang 2003). The superiority of the use of the two-particle method becomes rather explicit when the formulation and solution of the variational equations are troublesome. A practical problem one usually encounters is that, in general, one has to follow the orbit for quite a long time before obtaining a reliable LCE.

Hence the computation of LCEs for thousands of orbits is very expensive. In this case, the fast Lyapunov indicators (FLIs) of Froeschlé et al. (1997) are an ideal technique. The FLI means that the logarithm of the length of a tangential vector, which grows exponentially for a chaotic orbit, grows only polynomially for a regular motion. This allows one to quickly distinguish the two cases. Wu et al. (2006a) extended this idea and proposed the FLI with two nearby trajectories. Unlike the original approach of FLI (Froeschlé et al. 2000) with the tangential vector, the modification might fail to work without renormalization due to saturation of the orbits in a bounded chaotic region. To work out this problem, they introduced the renormalization technique to compute their FLI within a sufficiently long time span. It has proved successful to use the FLI to explore the global dynamics of phase space for a complicated relativistic system. Of course, there are other qualitative techniques for multidimensional systems, such as the power spectra, the frequency map analysis (Laskar 1994; Xie & Huang 2006), the smaller alignment index (Skokos 2004), the 0–1 test method (Gottwald & Melbourne 2004), and so on. For details, see a recent review in Wu & Huang (2005).

In a word, it is vital to choose a suitable numerical algorithm and chaos indicator as tools for the analysis of orbital dynamical evolution. As is stated above, one main motivation of the FLI with two nearby orbits presented by Wu et al. (2006a) is that it can be applied to complicated physical models. In the present paper, we shall deal with the other application of the FLI, that is, our objective is to ensure that numerical methods for the calculation of two nearby orbits are symplectic. As an illustration, in the computation of the LCE and FLI with the tangential vector, symplectic integrators can be used to solve the equations of motion for some Hamiltonian problems, while they are not a straightforward tool to treat the corresponding variational equations in general. For the Newtonian core-shell Hamiltonian system (Vieira & Letelier 1999) split into one important and one minor component, we consider the pseudo-order integrators to be one of the good integrators.

This paper is organized as follows. In Section 2 we mainly use two different orbits to evaluate the accuracy of one of the pseudo-order integrators (Laskar & Robutel 2001), which is applied to solve the Newtonian core-shell Hamiltonian system (Vieira & Letelier 1999). Then, we report on some applications of the FLI with two nearby orbits in Section 3. Finally, a summary follows in Section 4.

2 PHYSICAL MODELS AND NUMERICAL INTEGRATORS

First, we introduce the Newtonian core-shell model and the pseudo-8th-order symplectic integrator. Then, we estimate the relative energy errors and position errors of two different orbits (one may be regular, and the other, chaotic). As an in-depth exploration, we use LCEs, FLIs and Poincaré sections to independently check the classification of the two orbits.

2.1 Physical Models

It is possible to use static, relativistic core-shell systems to model black holes or neutron stars surrounded by axially symmetric massive additional matters such as shell and ring remnants in galaxies (Vieira & Letelier 1999). When the two conditions of weak field and slow motion of test particles in the vacuum between the core's horizon and the shell are satisfied, limiting cases of the relativistic models turn out to be the corresponding Newtonian counterparts, which could account for massive circumstellar dust shells

and rings around certain types of star remnants. The Newtonian potentials of the exterior shell are made up of multipoles from shell-like Legendre expansions. Because of the linear superposition of Newtonian potentials, the Newtonian core-shell system is expressible in cylindrical coordinates as

$$H = \frac{1}{2}(p_r^2 + p_z^2) + \frac{L^2}{2r^2} - \frac{1}{R} + Dz + \frac{Q}{2}(2z^2 - r^2) + \frac{O}{2}(2z^3 - 3zr^2), \tag{1}$$

where $R = \sqrt{r^2 + z^2}$, and the four parameters L, D, Q and O denote the angular momentum, dipole, quadrupole and octopole, respectively.

Obviously, in Cartesian coordinates Equation (1) can be changed into the following form:

$$\begin{aligned} H &= H_0 + H_1, \\ H_0 &= \frac{1}{2}(p_x^2 + p_y^2 + p_z^2) - \frac{1}{R}, \\ H_1 &= Dz + \frac{Q}{2}(2z^2 - x^2 - y^2) + \frac{O}{2}[2z^3 - 3z(x^2 + y^2)]. \end{aligned} \tag{2}$$

Besides the energy integral in Equation (2), there is always the angular momentum integral,

$$L = xp_y - yp_x. \tag{3}$$

In addition, we point out that the primary piece, H_0, is a Kepler part caused by the black hole; and the other, perturbing part, H_1, originating from the shell, though rather smaller, can not be neglected. For such systems, the pseudo-order symplectic integrators are very suitable.

2.2 Pseudo Eighth Order Symplectic Integrator

For convenience, Equation (2) is marked as $H = H_0 + \epsilon H_1$ with ϵ a small perturbation parameter. The Lie derivative with respect to H is denoted by $\mathcal{L}_H = \{H, \ \}$ ($\{\ ,\ \}$ being the Poisson bracket). We write $A = \mathcal{L}_{H_0}$ and $B = \mathcal{L}_{H_1}$. Clearly, the local truncation error in the Kernel of an nth-order symplectic integrator of Yoshida (1990) with a fixed time step τ is of $\mathcal{O}(\epsilon\tau^{n+1})$. Whereas a pseudo nth-order symplectic integrator of Chambers & Murison (2000) corresponds to its error in the form $\max\{\mathcal{O}(\epsilon^{\,2}\tau^3), \mathcal{O}(\epsilon\tau^{n+1})\}$. From the power of τ, the pseudo nth-order symplectic integrator seems to be a second-order standard symplectic integration scheme. However, it can achieve the accuracy of a nth-order symplectic integrator if $\mathcal{O}(\epsilon^{\,2}\tau^3)$ is sufficiently small. Otherwise, the error of the pseudo-order integrator still becomes much smaller than that of the conventional second-order symplectic integrator. Especially, a dramatic advantage the pseudo-order integrator has is that it contains only a combination of $n + 1$ Lie operators. Consequently, it has a greatly diminished roundoff errors and involves small computational cost, compared to the corresponding symplectic integrator.

Seen from the formal expression of error, the pseudo-order integrators do not necessary have a good accuracy when n becomes very large. In fact, Laskar & Robutel (2001) found that a pseudo sixth- or eighth-order symplectic integrator has the best numerical precision. Here we list the pseudo eighth-order integrator of the form

$$\mathrm{PS8} = e^{c_1\tau A} e^{d_1\tau\epsilon B} e^{c_2\tau A} e^{d_2\tau\epsilon B} e^{c_3\tau A} e^{d_2\tau\epsilon B} e^{c_2\tau A} e^{d_1\tau\epsilon B} e^{c_1\tau A}, \tag{4}$$

with the relevant coefficients,

$$\begin{aligned} c_1 &= \frac{1}{2} - \frac{1}{70}\sqrt{525 + 70\sqrt{3}}, \\ c_2 &= \frac{1}{70}(\sqrt{525 + 70\sqrt{3}} - \sqrt{525 - 70\sqrt{3}}\,), \\ c_3 &= \frac{1}{35}\sqrt{525 - 70\sqrt{3}}, \\ d_1 &= \frac{1}{4} - \frac{1}{72}\sqrt{30}, \\ d_2 &= \frac{1}{4} + \frac{1}{72}\sqrt{30}. \end{aligned}$$

Next, we shall apply the integrator in Equation (4) to Equation (2).

For simplicity, we consider only the case of a monopolar core plus shell octopoles. Let $D = 0$, $Q = 0$, energy $E = -3.147 \times 10^{-2}$, $L = 3.8$ and $O = 7.0129 \times 10^{-7}$. As far as initial conditions are concerned, $z = 0$ is always fixed, and p_z is a positive square root given by Equation (1). First, we take the starting point S (15.0, –0.015) (labeled as orbit S) in the r-p_r plane. Giving the transformation from the cylindrical coordinates to Cartesian coordinates, we work out Equation (2) by use of the method of Equation (4) with a fixed step-size of 1.0 (that is, the integration is always carried out in Cartesian coordinates). Figure 1A displays the relative energy error, which appears to consist of periodic changes instead of a secular growth with time. This shows that the integrator does preserve energy, which is an important property of symplectic integrators. For a different orbit with the initial point T (12.0, 0.040) (labeled as orbit T), we see an energy accuracy of the order of 10^{-8} (see Fig. 1B). However, the position errors $|\Delta \boldsymbol{r}|$ [1] of the two orbits are completely different. The error of orbit S (Fig. 1C) grows linearly with time and reaches the order of 10^{-3} at time 10^5, while the error of orbit T (Fig. 1D) apparently begins to grow exponentially at time 1.1×10^4. Why this difference? Answer: the two orbits may have different dynamical features.

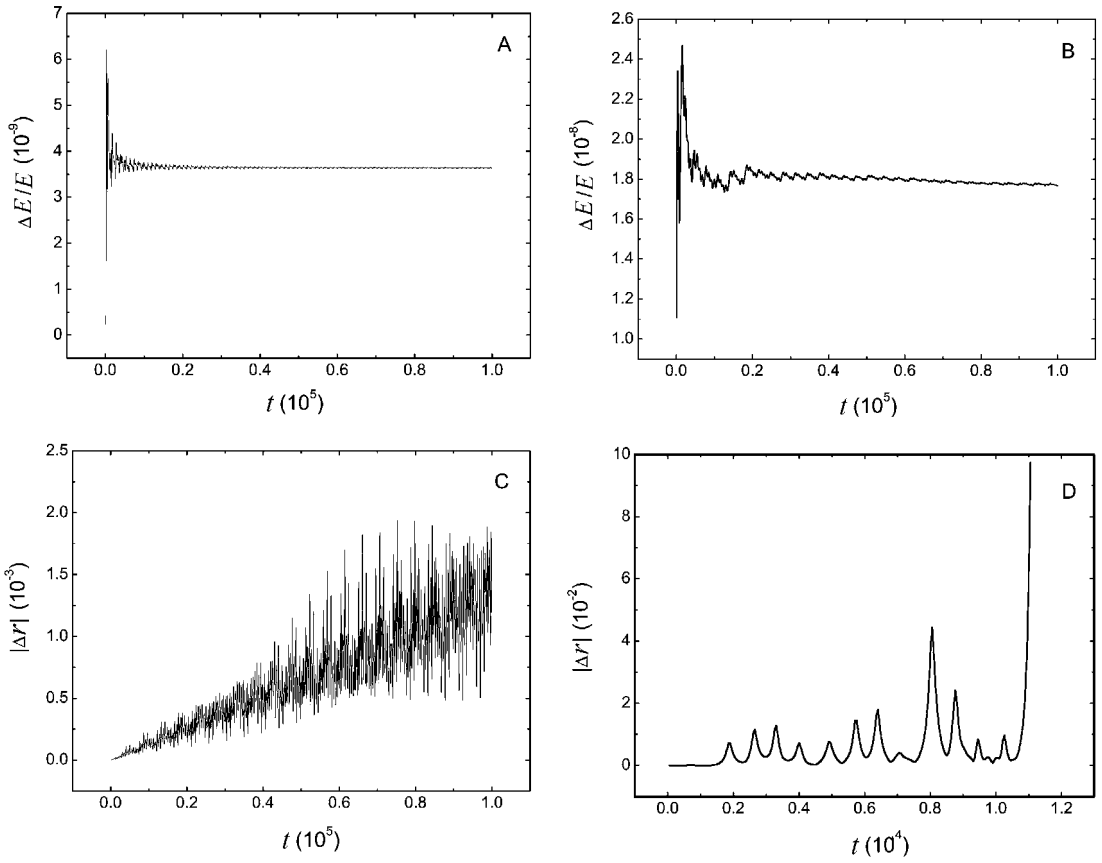

Fig. 1 Errors of the pseudo 8th symplectic integrator. Panels A and C represent the relative energy error and position error of orbit S, Panels B and D, those of orbit T.

[1] The related reference orbits are obtained from a 12th-order Cowell integrator.

2.3 Identifying the Classification of the Two Orbits

Now we use several methods to analyze the two orbits, the methods of LCEs, of FLI with two nearby orbits and of the Poincaré sections.

2.3.1 Lyapunov Characteristic Exponents

There are two methods for the calculation of the maximum LCE in published references. One is the so-called variational method with the expression

$$\begin{aligned} \lambda &= \lim_{t\to\infty} \varrho(t), \\ \varrho(t) &= \frac{1}{t} \ln \frac{|\boldsymbol{\xi}(t)|}{|\boldsymbol{\xi}(0)|}, \end{aligned} \tag{5}$$

where $\boldsymbol{\xi}(0)$ and $\boldsymbol{\xi}(t)$ stand for the tangential vectors in the phase space at the initial time and time t. The other is the two-particle method (Benettin et al. 1976) of the form,

$$\begin{aligned} \Lambda &= \lim_{t\to\infty} \chi(t), \\ \chi(t) &= \frac{1}{t} \ln \frac{d(t)}{d(0)}. \end{aligned} \tag{6}$$

In this equation, $d(t)$ is the distance in the phase space between two nearby trajectories with the initial separation $d(0)$. Tancredi et al. (2001) pointed out that it is best to choose $d(0)$ on the order of about 10^{-8}.

As mentioned above, the pseudo-order symplectic integrator of Equation (4) is very suitable for computing Equation (6). Figure 2 (left) plots the LCEs of the two orbits, S and T. As an illustration, we deal with the two orbits in the 3-dimensional system of Equation (2) for the calculation of the LCEs. In particular, the values of the LCEs are also checked with Equation (5) with an 8–9 order Runge-Kutta-Fehlberg algorithm of variable time-step (The same procedure was followed in the demonstrations below). In Figure 2, Curve A (for orbit S) decreases linearly with time towards zero. This seems to imply the regularity of orbit S. Curve B (for orbit T) does not seem to tend to a stable value even when the integration was carried to time 10^{7}. These facts show that the LCE is not very sensitive or quick to distinguish the dynamics of the two orbits. We now consider a more sensitive tool.

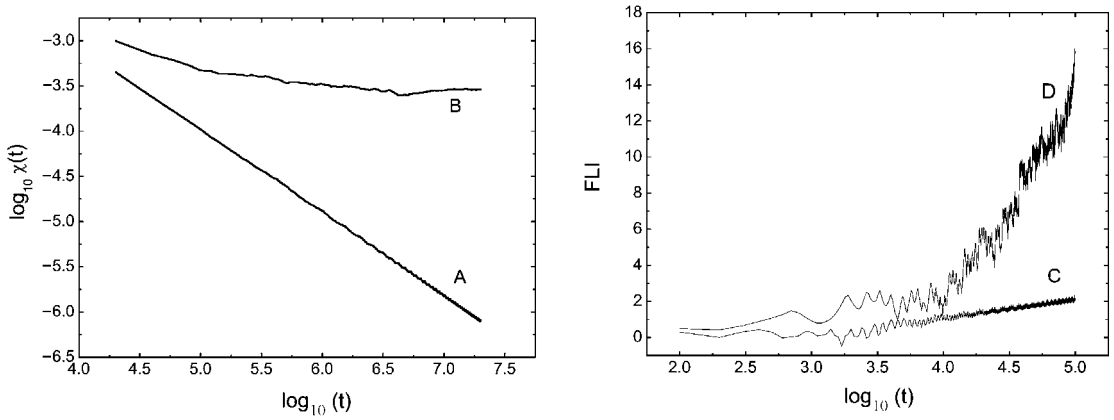

Fig. 2 Left panel: Curves A and B sketch the maximum Lyapunov characteristic exponents of orbits S and T, respectively. Right panel: Curves C and D correspond to the fast Lyapunov indictors of the two orbits.

2.3.2 The Fast Lyapunov Indictor based on two nearby orbits

Froeschlé & Lega (2000) used the tangential vector to construct the FLI as

$$\psi(t) = \log_{10} |\boldsymbol{\xi}(t)| \tag{7}$$

(the adopted logarithmic symbol is for the logarithm function in their article). Given a threshold, the indicator ψ tends to the value with completely different time rates for ordered and chaotic orbits: it varies more and more slowly for the former, while it does quickly for the latter, and it tends to different values for the two kinds of orbit in the same time interval. More specifically, it increases linearly with time ($\log_{10} t$) in the regular case, and exponentially in the chaotic case. This allows one to distinguish between the two cases.

In order to avoid using tangential vectors for complicated systems and consider the applicability of symplectic schemes, Wu et al. (2006a) developed the above idea and proposed the following form of FLI with two nearby orbits:

$$\mathrm{FLI}(t) = \log_{10} \frac{d(t)}{d(0)}. \tag{8}$$

Unlike Equation (7), Equation (8) has some difficulties in the computation if done without renormalisation. This is because the distance between the two orbits may expand so fast that it could reach the chaotic boundary and cause saturation. As a tentative solution to this problem, they gave a detailed algorithm of the FLI. Let $d(0) = 10^{-9}$. Saturation occurs when $d(t) = 1$, therefore $d(t) = 0.1$ can be chosen as a critical value for carrying out renormalization. Obviously, the number of renormalization for computing the FLI is less than that for the LCE. An advantage is to guarantee the speed of computation. Let k ($k = 0, 1, 2, \cdots$) be the sequential number of renormalization. The computation of the FLI satisfies the following requirement,

$$\mathrm{FLI}_k(t) = -k \cdot [1 + \log_{10} d(0)] + \log_{10} \frac{d(t)}{d(0)}, \tag{9}$$

where $d(0) \leq d(t) \leq 0.1$. Using this algorithm, we obtain the time variations of the FLIs of orbits S and T in the right panel of Figure 2. We find that the FLI for orbit S (Curve C) remain below 3.0 for integration time up to 10^5, while that of orbit T (Curve D) reaches 16.0 or so. Thus, Equation (8) provides a very sensitive tool to distinguish the regular orbit S from the highly chaotic orbit T. Also it may be noted that, in this chaotic case, the number of renormalizations is only two. By a comparison with the computed LCE in the left panel of Figure 2, we see that the FLI has a great merit in the identification of the orbital dynamical behavior. These results are again proved by the Poincaré sections (Fig. 3A). Here it is necessary to change the numerical solutions in Cartesian coordinate system to ones in the cylindrical coordinate system.

In short, now we can understand the contents of Figure 1. We note, further, that the indicator of Equation (8) is quick and sensitive to distinguish between chaos and ordered motion.

3 APPLICATIONS OF THE FLI WITH TWO NEARBY ORBITS

This section presents further applications of the FLI of Equation (8). Specifically, we shall know the behavior of the orbit by the variations of the FLI with a selected coordinate for fixed initial conditions and dynamical parameters. On the other hand, we try to find a relationship between the critical values of two parameters by tracing an orbit with the maximal radius $r_{\max}$ on the equatorial plane while the other initial conditions and dynamical parameters are fixed. Finally the global dynamical structure based on different values of the FLI is described.

3.1 Distribution of Regular and Chaotic Regions on a Straight Line

Similar to Wu et al. (2006a), we can find a distribution of regular and chaotic regions on the line $r = 13.5$ in Figure 3A. The detailed operation is as follow. Let the initial p_r range from –0.0763 to 0.0769 at intervals of 0.001, and all the dynamical parameters and the other initial conditions be fixed. Each of the initial orbits is numerically integrated up to time 10^5. Figure 3B plots the maximal value of FLI as a function of the initial action p_r. By a series of numerical experiments, we find that 7.5 is the critical value of FLIs between ordered and chaotic regions, that is, the orbit is regular when $\mathrm{FLI}_{\max} \leq 7.5$, and is chaotic if $\mathrm{FLI}_{\max} > 7.5$. Thus, three chaotic regions, [0.02869, 0.02969], [0.03969, 0.06769] and [0.07469, 0.07669], trapped in the straight line $r = 13.5$ are identified. Clearly, these results coincide with the results on the Poincaré sections. This shows the validity of the indictor of Equation (8).

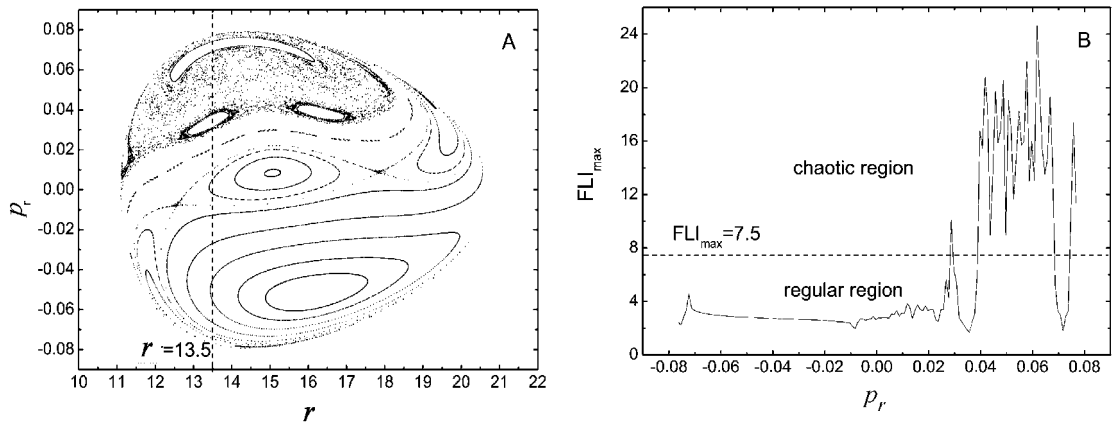

Fig. 3 Panel A: Poincáre section on the plane $z = 0$ with $p_z > 0$. Panel B: $\mathrm{FLI}_{\max}$ as a function of the initial value of p_r with fixed initial value of $r = 13.5$. Here regular and chaotic regions are identified on the basis of the differing values of FLIs.

3.2 The Transition from Regular Motion to Chaos

First we estimate effects on the dynamics of orbits of varying one dynamical parameter. For example, we fix the same parameters E and O (as in the above), and the same initial conditions $z = 0$ and $p_r = 0$, while vary L from 3.357 to 3.971. The initial value of r is the maximal root $r_{\max}$ of the equation $2Er^2 + 2r - L^2 = 0$. In practice, the chosen test orbit with $r_{\max}$ corresponds to the zero-velocity curve, called the critical line. Because of the effect of various perturbations, the dynamical characteristics (for example, stability and instability, regularity and chaos) in the critical line can easily vary, that is, the dynamical characteristics in the critical line are sensitively dependent on the variation of the dynamical parameters. Making use of these factors, Caranicolas & Papadopoulos (2003) used the critical line to discuss the transition from regular motion to chaos in elliptical galaxies. Here, we follow this method and establish a functional relation between the $\mathrm{FLI}_{\max}$ and L. This is shown in Figure 4A. The larger L gets, the weaker chaos becomes. This is because a large angular momentum means a large region of motion and hence a decreased gravity of the core on the test particle.

Similarly, we can draw two other diagrams: $\mathrm{FLI}_{\max}$—E (Fig. 4B), $\mathrm{FLI}_{\max}$—O (Fig. 4C). These plots show that the chaos emerges with increasing E or O. In fact, Figure 4C can be viewed as displaying the dynamical variation of the orbit with O when initial orbits vary over the parameters in Figures 4A and 4B.

Now let us survey some of the dynamical features yielded by the variation of two of the parameters at a time, the relationship between the two critical parameters. First consider that the parameter $L = 3.8$ is fixed, then we have $0 > E \geq -1/(2L^2) \approx -0.03462$ in the plane $z = 0$. Now let E run from –0.0334 to –0.0292, and let O range over interval $[10^{-7}, 10^{-6}]$. It should be noted that if $E+1/R-O/2\cdot[2z^3-3z(x^2+y^2)] < 0$ then as soon as O exceeds a certain value, we should stop the computing, give E the other value and begin the next part of integration.

Figure 5A displays the relationship between the critical values of O and E for the FLI, and clearly identifies the regular region and chaotic region. In addition, it clearly shows that larger energies (or octopolar parameter) correspond to stronger chaos. This result is physically quite reasonable. Similarly, Figure 5B plots the relationship between the critical Os and Ls. Here, we see that an increasing angular momentum corresponds to a weaker chaos. Unlike Caranicolas & Papadopoulos (2003), we cannot quite see a linear relationships between these two critical parameters. Without doubt, our method using the FLI is more convenient for finding the relationship than theirs, the method of Poincaré sections.

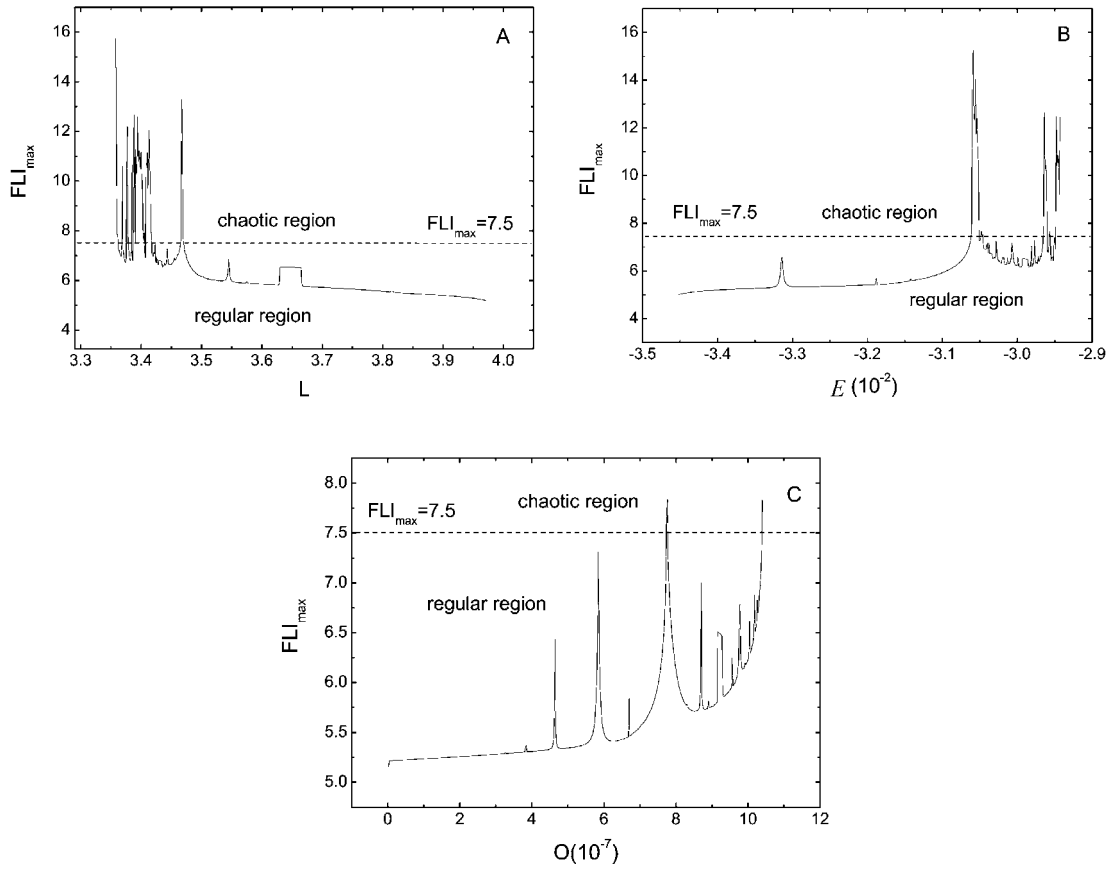

Fig. 4 Panels A, B and C: $\mathrm{FLI}_{\max}$ as a function of L, E, O, respectively. For each panel, two of three parameters $E = -0.03147$, $L = 3.8$ and $O = 7.0129 \times 10^{-7}$ are fixed. The initial variables are $z = p_r = 0$. The starting value of r is the $r_{\max}$ at the equatorial plane, and the initial value of p_z is given by Eq. (1).

3.3 The Global Structure of Phase Space

The many experiments above have shown that the indictor defined by Equation (8) is a perfect detector of chaos. Now we use it to draw the global structure of phase space of the core-shell system. We adopt the same dynamical parameters as Figure 3A. The chosen initial orbits for Equation (1) are as follows. We fix $z = 0$, and let r go from 11.1 to 20.3 in steps of 0.1. For every r, we have two roots $+p_r$ (> 0) and $-p_r$ (< 0) of the equation $p_r^2 = 2E - L^2/r^2 + 2/r$. Then we set p_r to run from $-p_r$ to $+p_r$ at steps of 0.001. Certainly, p_z (> 0) should satisfy Equation (1). Figure 6A plots all the starting points in the $r - p_r$ plane, where ordered and chaotic regions are distinguished according to the differing values of FLIs. As a result, Figure 6A resembles Figure 3A, apart from some details regarding the regular orbits. In addition, some black points in the regular regions mean onset of chaos. We also learn that the fraction of the chaotic region is 18.18%: this value was obtained by counting the number of chaotic points.

It should be emphasized that the FLI can be also used to study the global structure of phase space of the 3-dimensional system of Equation (2), while Poincaré sections cannot. For instance, we could fix $y = z = 0$ initially, and let the initial value of x (hence that of p_x) vary in a certain range. Note that the other initial conditions should satisfy the two integrals, Equations (2) and (3). Then we can easily construct Figure 6B, showing the regular and chaotic regions with a large number of initial points in the x-p_x plane.

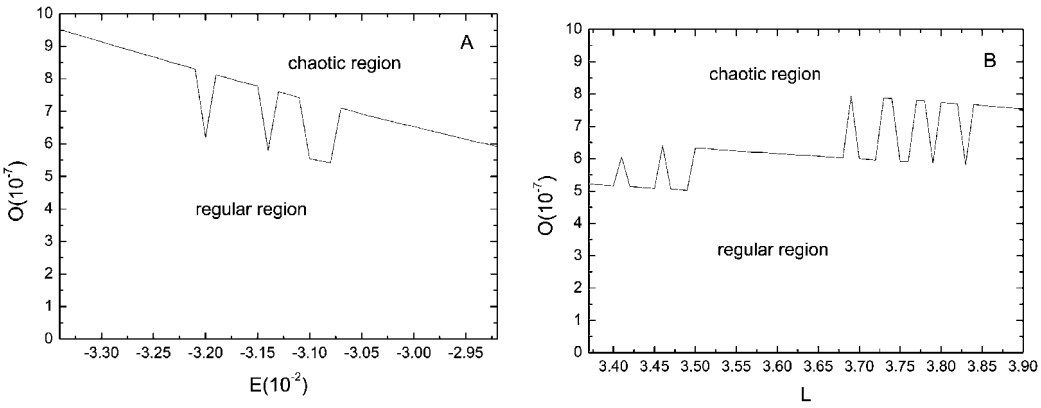

Fig. 5 Relationship between two selected critical parameters. Panel A: between E and O for fixed angular momentum $L = 3.8$. An orbit is chaotic or regular according as $\mathrm{FLI}_{\max}$ is greater or less than 7.5. As is shown, the larger the energy (or the octopolar parameter) is, the stronger chaos becomes. Panel B: Similar to panel A but for L and O with the fixed energy $E = -0.03147$.

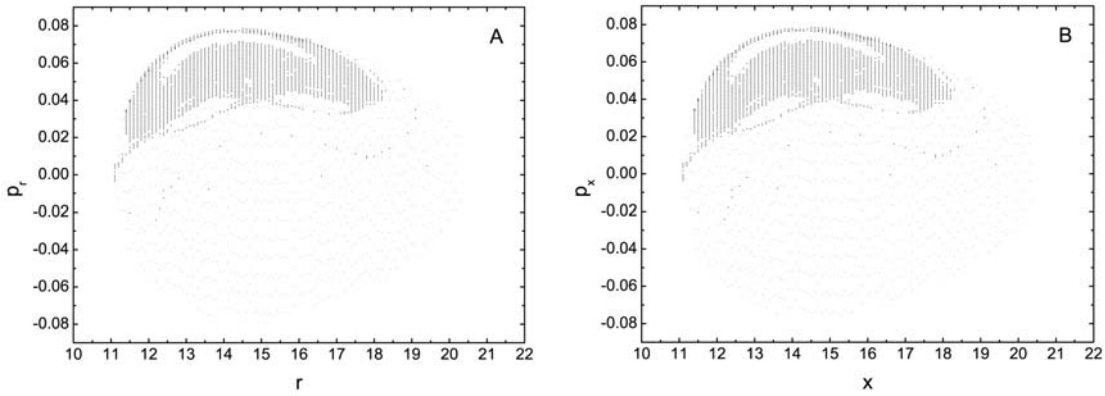

Fig. 6 Panel A: Initial points on the $r - p_r$ plane for the 2-dimensional system (1) define the regular regions (colored light gray) when $\mathrm{FLI}_{\max} \leq 7.5$, and the chaotic ones (colored black) with $\mathrm{FLI}_{\max} > 7.5$. Panel B: A set of initial points on the $x - p_x$ plane for the 3-dimensional system (2).

4 SUMMARY

We have used the pseudo 8th symplectic integrator to investigate the dynamics of orbits in the Newtonian core-shell system. This integrator is eminently suitable for calculating the two indictors of chaos: Lyapunov characteristic exponents and fast Lyapunov indictors with two nearby trajectories. One important point is to discuss some applications of the FLI in the analysis of chaos in the system. We can apply the FLI to obtain the regular and chaotic regions as one of the initial coordinate varies arbitrarily, and one is fixed by the energy integral, while the other initial variables and all the dynamical parameters are kept fixed. In addition, we are able to use it to explore the transition from regular motion to chaos. Specifically, it is interesting to use this indicator to estimate effects of varying one of the dynamical parameters on the dynamical behavior of the orbit. Further, we have explored relationships between two critical dynamical parameters, and find ordered and chaotic regions in two sides of the critical line relating the two parameters. Finally, the global structure of phase space of the 2-dimensional or 3-dimensional system is successfully characterized.

In sum, the fast Lyapunov indictor with two nearby trajectories is a simple, quick and sensitive tool to detect chaos from the regularity. A great merit of the indictor is that it can be conveniently used to treat complicated dynamical systems with many degrees of freedom. We plan to use it together with an appropriate numerical scheme to study relativistic gravitational systems or Newtonian n-body Hamiltonian problems in planetary dynamics in future work.

Acknowledgements We are grateful to the referee for her/his significant suggestions. This research is supported by the National Natural Science Foundation of China under Grant 10563001. It is also supported by Science Foundation of Jiangxi Province (0612034), Science Foundation of Jiangxi Education Bureau (200655), and the Program for Innovative Research Team of Nanchang University.

References

Baumgarte J., 1973, Celest. Mech., 5, 490
Benettin G., Galgani L., Strelcyn J.-M., 1976, Phys. Rev. A, 14, 2338
Caranicolas N. D., Papadopoulos N. J., 2003, New Astronomy, 9, 103
Chambers J. E., Murison M. A., 2000, AJ, 199, 425
Contopoulos G., Barbanis B., 1989, A&A, 222, 329
Froeschlé C. L., Lega E., Gonczi R., 1997, Celest. Mech. Dyn. Astron., 67, 41
Froeschlé C. L., Lega E., 2000, Celest. Mech. Dyn. Astron., 78, 167
Gottwald G. A., Melbourne I., 2004, Proc R. Soc. London. Ser. A, 463
Laskar J., 1994, A&A, 287, 9
Laskar J., Robutel Ph., 2001, Celest. Mech. Dyn. Astron., 80, 39
Liu F.-Y., Wu X., Lu B.-K., 2006, Chinese Astron. Astrophys., 30, 87
Nacozy P. E., 1971, Ap&SS, 14, 40
Skokos Ch., 2004, J. Phys. A, 37, 6269
Tancredi G., Sánchez A., Roig F., 2001, AJ, 121, 1171
Vieira W. M., Letelier P. S., 1999, ApJ, 513, 383
Wisdom J., Holman M., Touma J., 1991, AJ, 102, 1528
Wu X., He J. Z., 2006, Int. J. Mod. Phys. C, 17, 1613
Wu X., Huang T.-Y., 2003, Phys. Lett. A, 313, 77
Wu X., Huang T.-Y., 2005, Progress in Astronomy, 23(4), 318 (in Chinese)
Wu X., Huang T.-Y., Wan X.-S., Zhang H., 2007, AJ, 313, 2643
Wu X., Huang T.-Y., Zhang H., 2006a, Phys. Rev. D, 74, 083001
Wu X., Zhang H., 2006, ApJ, 652, 1466
Wu X., Zhang H., Wan X. S., 2006b, Chin. J. Astron. Astrophys. (ChJAA), 6, 125
Wu X., Zhu J. F., He J. Z., Zhang H., 2006c, Comput. Phys. Commun., 175, 15
Xie Y., Huang T.-Y., 2006, Chin. J. Astron. Astrophys. (ChJAA), 6, 705
Yoshida H., 1990, Phys. Lett. A, 150, 262